

# VeLU: Variance-enhanced Learning Unit for Deep Neural Networks

Ashkan Shakarami<sup>1</sup>, Yousef Yeganeh<sup>2</sup>, Azade Farshad<sup>2</sup>, Lorenzo Nicolè<sup>1</sup>,  
Stefano Ghidoni<sup>1</sup>, Nassir Navab<sup>2</sup>

<sup>1</sup>University of Padova, Italy

<sup>2</sup>Technical University of Munich, Germany

{ashkan.shakarami, lorenzo.nicole}@phd.unipd.it, stefano.ghidoni@unipd.it  
{y.yeganeh, azade.farshad, nassir.navab}@tum.de

## Abstract

Activation functions are fundamental in deep neural networks and directly impact gradient flow, optimization stability, and generalization. Although ReLU remains standard because of its simplicity, it suffers from vanishing gradients and lacks adaptability. Alternatives like Swish and GELU introduce smooth transitions, but fail to dynamically adjust to input statistics. We propose VeLU, a Variance-enhanced Learning Unit as an activation function that dynamically scales based on input variance by integrating ArcTan-Sin transformations and Wasserstein-2 regularization, effectively mitigating covariate shifts and stabilizing optimization. Extensive experiments on ViT\_B16, VGG19, ResNet50, DenseNet121, MobileNetV2, and EfficientNetB3 confirm VeLU's superiority over ReLU, ReLU6, Swish, and GELU on six vision benchmarks. The codes of VeLU are publicly available on [GitHub](#).

**Keywords:** Activation function, Deep Neural Networks, Optimal Transport, Wasserstein-2 regularization.

## 1 Introduction

Activation functions are crucial in deep learning, shaping optimization, gradient propagation, and generalization. The Rectified Linear Unit (ReLU) [1, 2] has long been the standard choice due to its simplicity and computational efficiency. However, ReLU suffers from the *dying neuron* problem, where inactive units cease to update during training. To address this limitation, variants such as Leaky ReLU [3], PReLU [59], and ELU [4] have been proposed, allowing small negative activations to preserve gradient flow.

Recent advancements introduced smooth, non-monotonic activation functions, such as Swish [18] and GELU [5], which enhance optimization and generalization. These functions, however, apply the same transformation regardless

of input statistics, limiting their adaptability to varying activation distributions across network layers. To address this, adaptive activation methods such as Dynamic ReLU [60], introduce input-dependent behavior or learnable parameters. While effective, these approaches often incur computational overhead due to added trainable parameters.

Although several variations of ReLU, Swish, and adaptive functions exist [8, 18], our goal is to develop a robust activation function that combines non-linearity, adaptivity, and statistical alignment—without increasing model complexity. Therefore, this paper introduces VeLU, a Variance-enhanced Learning Unit that dynamically adjusts its response based on input variance, offering an adaptive activation function.

Unlike conventional activation functions, VeLU reduces internal covariate shifts [9], which refer to undesirable changes in the distribution of activations between layers during training caused by input shifts, and ensures stable optimization across layers and architectures. These characteristics—namely reduced activation drift and improved training stability—are particularly beneficial in deep networks such as CNNs and ViTs, where the activation distributions vary significantly.

VeLU achieves these improvements by integrating ArcTan-Sin transformations, which combine arctangent and arcsine functions to introduce smooth, bounded non-linearity, aiding gradient flow and preventing saturation. Furthermore, it incorporates Wasserstein-2 regularization, an Optimal Transport (OT) technique that minimizes the Wasserstein-2 distance [11], aligning the activation distribution with a Gaussian prior to enhance representation stability and generalization. While OT has been applied in domain adaptation and generative modeling [29], its integration into activation design remains underexplored (It is, indeed, a mathematical framework that determines the most efficient way to morph one probability distribution into another. Originally rooted in logistics and resource allocation, OT quantifies the minimal *cost* required to move probability mass from one distribution to match another, where the cost is typically based on a distance metric such as the Euclidean or Wasserstein-2 distance [15, 16]).

Extensive experiments on benchmark datasets—including CIFAR-10, CIFAR-100, MNIST, Fashion-MNIST, Corel-1K, and Corel-10K—demonstrate that VeLU outperforms ReLU, ReLU6, Swish, and GELU across multiple architectures, including ViT B16, VGG19, ResNet50, DenseNet121, MobileNetV2, and EfficientNetB3 [12, 13]. These results establish VeLU as a scalable and effective alternative to conventional activation functions in deep neural networks.

## 2 VeLU

### 2.1 Structure

Mathematically, VeLU is defined as Equation 1, where  $\sigma(x)$  is the sigmoid function that ensures smooth non-linearity, while  $\lambda$  is a trainable scaling parameter

allowing dynamic adaptability. The terms  $\alpha, \beta_1, \beta_2, \gamma$ , and  $\mu$  are hyperparameters that control the shape and response of the function, providing additional flexibility. These parameters— $\alpha, \beta_1, \beta_2, \gamma$ , momentum, and  $\lambda_{OT}$ —jointly influence the non-linearity, adaptiveness, and regularization behavior of VeLU, and require careful tuning to ensure stable and effective model training. In the following, we provide a detailed description of each parameter (In [section 3](#), the selection of hyperparameter values is explained, as well).

$$f(x) = \lambda \cdot x \cdot \sigma \left( \alpha \cdot \left( \tan^{-1}(\beta_1 x) + \sin^{-1}(\beta_2 x) \right) \right) \cdot \left( 1 + \gamma \cdot \tanh(\mu \cdot \sigma_x) \right) - \lambda_{OT} \cdot W_2(x, \mathcal{N}(0, 1)). \quad (1)$$

**Scaling Parameter ( $\alpha$ ):** This parameter controls the strength of the non-linearity in the activation function. It modulates the sigmoid activation applied to the transformed input, influencing how sharply the function transitions between different input values. A higher  $\alpha$  value enhances non-linearity, while lower values produce smoother transitions.

**Transformation Parameters ( $\beta_1$  and  $\beta_2$ ):** These parameters govern the interaction of trigonometric transformations within the activation function. Specifically,  $\beta_1$  scales the input for the arctangent transformation, while  $\beta_2$  scales the input before applying arcsin. As for their effects, larger values of  $\beta_1$  and  $\beta_2$  amplify the non-linearity of their respective functions, resulting in sharper activation responses. Conversely, smaller values suppress these non-linear characteristics, causing the activation to behave more linearly. This tunability enables fine-grained control over how gradually or aggressively the activation responds to input variations.

**Adaptive Scaling Factor ( $\gamma$ ):** The parameter  $\gamma$  adjusts the adaptability of the activation function based on the input variance. It controls the impact of the standard deviation of input activations via a hyperbolic tangent function. Higher values of  $\gamma$  allow the activation function to dynamically adjust its response based on input statistics, leading to more flexible feature transformations.

**Momentum Parameter (momentum):** This parameter influences the smoothing effect of the adaptiveness term. It works in conjunction with  $\gamma$ , determining how much the function scales its response based on the statistical properties of the input. A higher momentum value increases the sensitivity to input variations.

**Wasserstein Regularization Weight ( $\lambda_{OT}$ ):** This parameter controls the contribution of the Wasserstein regularization term, which ensures that the dis-

tribution of activation outputs remains close to a predefined Gaussian distribution. Higher values  $\lambda_{OT}$  enforce stronger regularization, potentially improving generalization but also risking instability if set too high.

## 2.2 Visual behavior

Figure 1 visualizes the behavior of VeLU under different parameter configurations, illustrating how hyperparameters such as  $\alpha$ ,  $\beta_1$ ,  $\beta_2$ ,  $\gamma$ , and  $\mu$  influence the shape of the activation function. The parameter  $\alpha$  controls the steepness of the sigmoid term, determining the rate at which the activation transitions [18, 5]. The components  $\tan^{-1}(\beta_1 x)$  and  $\sin^{-1}(\beta_2 x)$  introduce a distinctive combination of non-linearities, setting VeLU apart from other activation functions that rely on traditional ReLU-based formulations [17].

Furthermore, the variance-based term ( $\sigma_x$ ) allows dynamic adaptation based on the input distribution, ensuring stability while preventing saturation or vanishing gradients[9, 14]. The Wasserstein regularization term also ensures that the activation output distribution aligns with a Gaussian target, further stabilizing the training and reducing the impact of internal covariate shifts[11, 29].

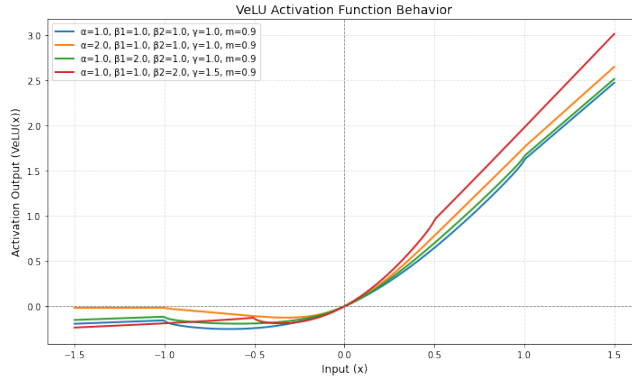


Figure 1: Visualization of the VeLU Activation Function Behavior under different parameter configurations. The plot highlights VeLU’s smoothness, non-linearity, and adaptability to various parameterizations, making it practical for deep neural network architectures, including CNNs and ViTs [6, 7].

In Figure 2, VeLU is compared with ReLU, Swish, and GELU, providing a direct visualization of their respective behaviors in the input range  $[-1.5, +1.5]$ . ReLU exhibits a sharp transition at  $x = 0$ , which can lead to sparse gradient updates and neuron death [1, 19]. Swish [18] and GELU [5], on the other hand, are smooth and unbounded above, promoting better gradient flow and improved generalization [20], but lack dynamic variance-adaptive scaling inherent to VeLU.

In contrast, VeLU offers a more flexible and adaptive response, maintaining smooth transitions while incorporating self-adaptive scaling and boundedness

below [17]. The OT component further reduces internal covariate shifts, improving the expressiveness of features across layers [29, 15]. This comparison highlights VeLU’s ability to combine the strengths of existing activation functions while addressing their limitations. In addition, its self-adaptive properties improve training stability and convergence in deep networks, allowing robust performance, better gradient flow, and enhanced generalization, especially in complex data distributions encountered in CNNs [6] and ViTs [7]. The ablation experiments and various experiments conducted in [section 3](#) demonstrate the aforementioned advantages of VeLU.

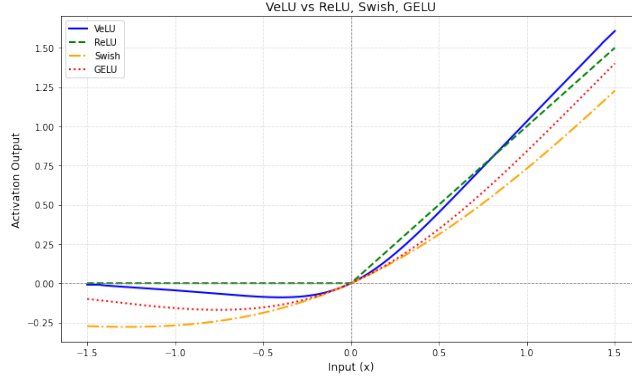


Figure 2: Comparison of VeLU with standard baseline activation functions.

### 2.3 Mathematical characteristics

VeLU exhibits a **non-monotonic response** because the ArcTan-Sin formulation introduces a smooth transition between positive and negative inputs. Unlike ReLU, which thresholds negative values at zero [1, 19], VeLU retains small negative activations, helping to propagate the gradient and prevent neuron death [59, 21]. VeLU also dynamically scales based on the input distribution, addressing limitations of static activation functions such as ReLU and Swish [18].

The **variance-based scaling factor** in VeLU adjusts the activations proportionally to the standard deviation  $\sigma_x$ , ensuring stable gradient flow and robustness across layers [17]. This adaptation is given by [Equation 2](#), where  $\gamma$  and  $\mu$  are hyperparameters controlling the sensitivity of adaptation.

$$s_{\text{adaptive}} = 1 + \gamma \cdot \tanh(\mu \cdot \sigma_x), \quad (2)$$

To further stabilize training, VeLU incorporates **Wasserstein-2 distance minimization** between its output distribution and a Gaussian target [11, 15], shown in [Equation 3](#). This forces activations to maintain well-conditioned distributional properties, reducing internal covariate shifts [29] and improving optimization.

$$W_2^2 = (E[x] - \mu)^2 + (\sigma_x - \sigma_{\text{target}})^2. \quad (3)$$

In neural networks, preactivations refer to the intermediate values computed by each neuron before applying the non-linear activation function—that is, the output of the linear transformation  $Wx + b$ . Studying their distribution helps assess how well the network maintains activation flow across layers [10]. Figure 3 illustrates the distribution of preactivations before and after training ResNet50 using VeLU. In this figure, the histogram displays the frequency distribution of preactivation values from a representative hidden layer, comparing the network’s behavior at initialization and after convergence. As shown, the post-training distribution is more concentrated and symmetric, suggesting that VeLU helps stabilize activation dynamics during training. This stabilization reduces fluctuations that contribute to internal covariate shift, a well-known challenge in deep learning models [9, 14]. By promoting a more structured activation distribution, VeLU facilitates improved gradient flow, which can enhance optimization efficiency and model convergence (Table 1) [6, 7]. This effect results in a more well-conditioned loss landscape, mitigating abrupt activation transitions commonly observed in functions such as ReLU.

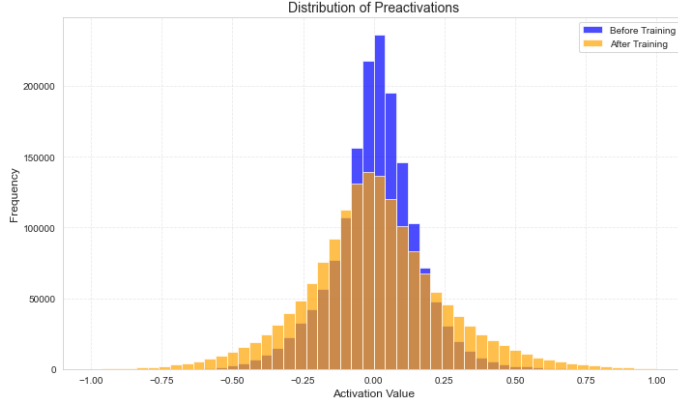


Figure 3: Histogram of preactivation values from a hidden layer in ResNet50, before and after training with VeLU. The post-training distribution is more concentrated and symmetric, indicating improved activation stability.

## 2.4 Smoothness and Adaptability

The smooth and adaptive nature of VeLU facilitates more efficient gradient propagation in deep networks by addressing limitations found in traditional activation functions. Unlike ReLU, which is continuous but non-differentiable at zero due to a sharp kink in its graph, VeLU maintains a continuously differentiable structure, promoting stable weight updates and improving network expressivity.

The **first derivative** of VeLU, given in Equation 4, exhibits two key properties that contribute to retaining large gradients over a broader input range. First, the term involving the derivative of the sigmoid function ( $\sigma'$ ) ensures a non-zero gradient even for moderately large inputs, in contrast to ReLU, which has zero gradients for negative values. Second, the inclusion of the hyperbolic secant squared function ( $\text{sech}^2$ ), which peaks at zero and smoothly decays for extreme values, allows VeLU to maintain a significant gradient magnitude over a wider range of activations compared to sigmoid and tanh, where gradients diminish sharply for large positive and negative inputs.

$$f'(x) = \lambda \cdot \sigma' \cdot s_{\text{adaptive}} + f(x) \cdot \gamma \cdot \mu \cdot \text{sech}^2(\mu \cdot \sigma_x), \quad (4)$$

This gradient-preserving property facilitates efficient information flow during backpropagation, particularly in deep architectures, where it helps mitigate the vanishing gradient problem. By maintaining a more stable and well-conditioned loss landscape (defined as the surface created by mapping the loss value over the model’s parameter space), VeLU promotes smoother gradients and fewer abrupt changes in curvature during optimization. This results in more efficient and reliable training, as the optimizer can navigate toward minima more effectively without getting stuck in sharp or irregular regions, which are often associated with unstable learning.

Besides, smoothness is crucial for optimizing and generalizing neural networks [6, 22]. Figure 4 plots the ResNet50 output landscape with different activation functions. The output landscape resulting from ReLU (Figure 4a) exhibits sharp and distinct regions, potentially caused by its non-smooth nature and abrupt transitions at  $x = 0$  [1, 19]. GELU (Figure 4c) and Swish (Figure 4b) show smoother landscapes compared to ReLU, which improve gradient flow [5, 18] but lack any adaptive scaling based on the input distribution. In contrast, VeLU (Figure 4d) provides a smooth and adaptive landscape, characterized by gradual transitions and the ability to dynamically adjust activations based on input variance, a property that helps mitigate sharp loss surfaces and improve optimization stability [23].

Therefore, the smoothness of VeLU’s output landscape directly impacts the loss landscape, making it more well-conditioned and stable during optimization [22, 24]. By dynamically adapting to the input distribution and incorporating Wasserstein-2 regularization [11], VeLU ensures that the activation distributions remain well-behaved throughout training, mitigating internal covariate shifts [9]. This reduces sensitivity to initialization and learning rates [25], allowing VeLU to perform consistently well across different architectures and datasets. Furthermore, OT-based alignment with Gaussian priors enhances gradient flow and regularization [26], fostering faster convergence and improved robustness in deep networks. As demonstrated in Section 3, VeLU offers considerable improvements in stability, convergence, and generalization compared to existing activation functions [5, 18] by combining self-adaptive scaling, smooth non-linearity, and distributional control.

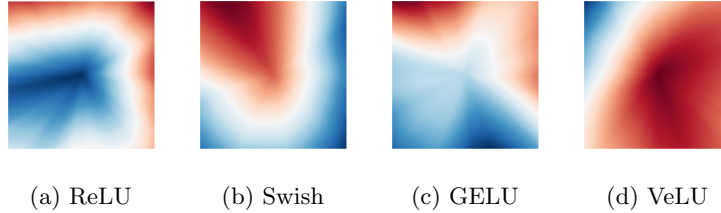


Figure 4: The output landscape of a ResNet50 with different activation functions. The figure is generated by passing two scalars, the  $x$  and  $y$  coordinates of each position in a grid, into a randomly initialized ResNet50 that outputs a single scalar. ReLU has sharp transitions, whereas Swish and GELU offer smoother landscapes. VeLU, with higher smoothness and adaptability, enhances optimization stability and generalization.

### 3 Experiments

We evaluated VeLU’s performance by comparing it with standard activation functions, including ReLU [1], Swish [18, 36], ReLU6 [30] and GELU [5, 7], across multiple deep learning architectures and benchmark datasets.

The evaluation was carried out under two scenarios: (1) partial replacement of activation functions and (2) full replacement of a model’s activation functions with VeLU. In the first scenario, VeLU was integrated into the model classification head (the final layers), leaving the feature extraction backbone unchanged. This setup allowed us to verify VeLU compatibility with other activation functions in the backbone, which is particularly important for fine-tuning pre-trained models [27]. Our experiments followed this scenario, except for those presented in Table 5 and Table 6, where we applied the second scenario, replacing all activation functions in ResNet50 [6] and the final added layers with VeLU. This demonstrated that VeLU can work as the primary activation function in a neural network without requiring additional activation functions.

For convolutional models (e.g., ResNet [6], VGG [28], MobileNet [30], and DenseNet [13]), we employed a global average pooling layer [31] to condense spatial features before feeding them into the classifier. In contrast, we omitted the pooling step for ViT\_B16 [7], which outputs a 2D feature vector. The classifier consisted of two fully connected layers with 256 and 64 neurons, each followed by an activation function. The final layer was a softmax classifier that mapped the learned representations to class probabilities. This structure enabled a standardized evaluation of VeLU across various architectures.

We conducted our experiments on widely used computer vision benchmarks, including CIFAR-10, CIFAR-100 [32], MNIST [33], Fashion-MNIST [34], Corel-1K, and Corel-10K [35]. Although these benchmarks are relatively classical, they remain standard for evaluating activation functions because of their controlled complexity, ease of reproducibility, and broad adoption in the literature. Moreover, several recent activation function studies (e.g., Swish [18] and GELU [5])



have also used these datasets, ensuring fair and meaningful performance comparisons.

In the data division for creating the training and validation sets, we followed the benchmark rules, which means we used the training and val/test sets of the benchmarks as they are. Besides, we used a random data selection approach with an 80% training and 20% test split for Corel-1K and Corel-10K. To ensure a fair comparison, we kept the learning rate schedules and other hyperparameters consistent across all activation functions in the model training. Each model was trained for 5 to 20 epochs, depending on the network’s depth and convergence needs. We then report the mean accuracy, loss, training time, inference speed, and memory usage.

Although we provided default initial values for VeLU parameters in our public code implementation on [GitHub](#) and a guideline for **parameter selection and stability considerations**, they can also be adjusted according to the specific task. This flexibility can be advantageous, as it allows for task-specific optimization [49], improved generalization [25], and adaptability to different architectures [36]. However, it can also introduce challenges such as increased complexity in manual tuning [50], task sensitivity [51], and computational overhead [52]. To address these issues, we propose the integration of an automated hyperparameter optimization module as a future improvement, which can dynamically set the best initial values based on a sample of input data [53]. Potential approaches include Bayesian optimization [54], gradient-based meta-learning [55], hyperparameter search algorithms (e.g., Optuna [56], Hyperopt [57], and KerasTuner [58]). This improvement can improve VeLU’s usability and efficiency in different deep-learning tasks while reducing the need for manual tuning.

**Guidelines on Parameter Selection and Stability Considerations:** The performance and stability of the VeLU depend on the careful tuning of its parameters:  $\alpha$ ,  $\beta_1$ ,  $\beta_2$ ,  $\gamma$ , momentum, and  $\lambda_{OT}$ . Increasing these parameters, particularly  $\alpha$  and  $\beta$  values, leads to sharper activation responses, which may result in gradient explosion and NaN losses during training. To prevent this, users should implement gradient clipping in the optimizer (e.g., setting `clipnorm=1.0` or `clipvalue=0.5`) to stabilize weight updates. Additionally, the computation of the adaptive scaling factor involves the operation:

$$\text{std\_dev} = \frac{1}{\sqrt{\mathbb{E}[x^2] + \epsilon}}. \quad (5)$$

To prevent numerical instability, another recommendation is to use a slightly larger  $\epsilon$  value (e.g.,  $10^{-3}$  instead of  $10^{-6}$ ). When modifying  $\gamma$ , which influences the adaptive response, it is advisable to clamp the adaptive factor within a controlled range using Equation 6. This ensures that the scaling effect remains within a reasonable range, preventing excessively large activation values.

$$\text{adapt\_factor} = \text{clip}(1 + \gamma \cdot \tanh(\text{std\_dev} \cdot \text{momentum}), 0.5, 2.0). \quad (6)$$

Furthermore, the Wasserstein regularization term  $\lambda_{OT}$  should be chosen carefully. A high  $\lambda_{OT}$  value forces activations towards a Gaussian target distribution, which may interfere with model convergence and cause unstable gradients. If training diverges, users should try reducing  $\lambda_{OT}$  (e.g., from 0.1 to 0.01 or 0.001) to balance regularization without adversely affecting learning dynamics. In summary, when experimenting with large parameter values, users should:

- Apply gradient clipping (`clipnorm=1.0` or `clipvalue=0.5`).
- Use a larger epsilon in the standard deviation calculation ( $\epsilon = 10^{-3}$ ).
- Clamp `adapt_factor` to a safe range ( $0.5 \leq \text{adapt\_factor} \leq 2.0$ ).
- Reduce  $\lambda_{OT}$  if training instability occurs.

By following these guidelines, users can safely explore different VeLU configurations while maintaining numerical stability and convergence reliability.

### 3.1 Evaluation of VeLU across Architectures

Table 1 compares VeLU with standard activation functions across diverse architectures, including CNNs [33, 2] and ViTs [7]. Across all models, VeLU consistently improves top-1 accuracy, confirming its adaptability to both convolutional and transformer-based architectures.

Notably, performance gains are especially pronounced in deeper or residual architectures such as ResNet50 and DenseNet121, where VeLU enhances top-1 accuracy by nearly 2%, suggesting improved gradient flow and stability. In lightweight models like MobileNetV2, even modest gains indicate VeLU’s suitability under parameter-constrained conditions. ViT-B16 also benefits, where VeLU outperforms GELU in both top-1 and top-5 metrics, highlighting its compatibility with self-attention mechanisms.

These results suggest that VeLU delivers generalizable improvements across architectures with varying depth, connectivity, and inductive biases, supporting its use as a versatile alternative to standard activations.

### 3.2 Evaluation of VeLU Across Benchmarks

Table 2 compares MobileNetV2 [12] with and without VeLU across diverse datasets. The results consistently show that integrating VeLU improves top-1 accuracy across all benchmarks, especially in fine-grained and multi-class datasets such as CIFAR-100 and Corel-1K.

In CIFAR-100 and Corel-10K, VeLU yields notable gains in both top-1 and top-5 accuracy, indicating improved feature discrimination in more complex classification tasks. The method also achieves perfect top-5 accuracy on MNIST and Corel-1K, reflecting enhanced confidence in prediction certainty. Even in cases where baseline top-5 performance remains high (e.g., CIFAR-10, Fashion-MNIST), VeLU delivers modest improvements in top-1 accuracy.

Table 1: Performance comparison of various architectures with and without VeLU. Accuracy (%) and Top-5 Accuracy (%) are reported.

Model	Activation	Top-1 Acc (%)	Top-5 Acc (%)
EfficientNetB3	VeLU	<b>87.61</b>	<b>99.40</b>
	Swish [18]	87.18	99.22
VGG19	VeLU	<b>90.97</b>	99.71
	ReLU [8]	90.30	<b>99.82</b>
ResNet50	VeLU	<b>91.27</b>	99.41
	ReLU [8]	89.44	<b>99.61</b>
MobileNetV2	VeLU	<b>91.32</b>	99.70
	ReLU6 [30]	90.69	<b>99.77</b>
DenseNet121	VeLU	<b>91.85</b>	<b>99.49</b>
	ReLU [8]	89.99	99.38
ViT_B16	VeLU	<b>96.25</b>	<b>99.95</b>
	GELU [5]	95.80	99.87

Overall, these results highlight VeLU’s effectiveness in boosting performance across tasks of varying complexity, making it a robust choice for deep learning applications requiring both accuracy and generalization.

Table 2: Performance comparison of the Baseline model with and without VeLU across various benchmarks. Accuracy (%) and Top-5 Accuracy (%) are reported. The original Baseline results are referenced from [12].

Benchmark	Model	Top-1 Acc (%)	Top-5 Acc (%)
CIFAR-10 [32]	Baseline	90.69	<b>99.77</b>
	<b>VeLU in Baseline</b>	<b>91.32</b>	99.70
CIFAR-100 [32]	Baseline	71.05	91.54
	<b>VeLU in Baseline</b>	<b>72.63</b>	<b>92.36</b>
MNIST [33]	Baseline	99.01	99.99
	<b>VeLU in Baseline</b>	<b>99.21</b>	<b>100</b>
Fashion-MNIST [34]	Baseline	91.10	<b>99.75</b>
	<b>VeLU in Baseline</b>	<b>91.13</b>	99.50
Corel1K [48]	Baseline	91	99
	<b>VeLU in Baseline</b>	<b>93.50</b>	<b>100</b>
Corel10K [48]	<b>Baseline</b>	86.45	95.70
	VeLU in Baseline	<b>87.90</b>	<b>97.50</b>

Table 3 presents the Top-1 accuracy results of ResNet50 [6] with VeLU across multiple benchmark datasets, along with the relative accuracy gain compared to the original activation function. The results demonstrate a consistent improvement in classification performance, with VeLU yielding notable gains in all cases. This table corresponds to the full replacement of activation functions in ResNet50 with VeLU, following the second scenario described in section 3. The

most significant improvement is observed in Corel-1K [39] (+9.00%), followed by Corel-10K (+3.85%) and CIFAR-100 [32] (+3.12%), indicating that VeLU effectively enhances feature extraction and decision boundaries in datasets with high variability. For CIFAR-10 (+1.90%), Fashion-MNIST [34] (+0.66%), and MNIST [33] (+0.36%), the gains, while smaller, still highlight VeLU’s ability to improve classification accuracy.

The overall trend suggests that VeLU benefits datasets with complex structures and higher intra-class variations, as seen in the Corel datasets and CIFAR-100. Meanwhile, for simpler datasets such as MNIST, the accuracy gain is less pronounced, likely due to the already high baseline performance [33]. These findings reinforce VeLU’s suitability as an activation function that enhances model generalization.

Table 3: Performance of VeLU in ResNet50 across benchmarks (The full activation replacement with VeLU). Accuracy (Acc) and Gains are reported.

Benchmark	Acc (%)	Gain
CIFAR-10	91.29	<b>+1.90</b>
CIFAR-100	72.07	<b>+3.12</b>
MNIST	99.34	<b>+0.36</b>
Fashion-MNIST	92.26	<b>+0.66</b>
Corel1K	93.50	<b>+9.00</b>
Corel10K	87.35	<b>+3.85</b>

Figure 5 presents the validation accuracy (left) and validation loss (right) for ResNet50 [6] trained with VeLU (blue) and the original activation function (orange) over 20 epochs. The results indicate that the VeLU-based model consistently achieves higher validation accuracy across all epochs. In particular, in the initial training phase, both models exhibit a rapid increase in accuracy, but the VeLU-based model maintains a higher performance after a few epochs, stabilizing at a higher accuracy level by the final epochs. The validation loss curves further support this observation. Initially, the loss for both models decreases sharply, with VeLU showing a slightly higher loss at the very beginning. However, as training progresses, the loss for the VeLU-based model stabilizes to a lower value than the original activation function, suggesting improved convergence and better generalization [40, 41]. VeLU’s consistently lower validation loss in the later epochs highlights its potential to reduce overfitting while improving model robustness.

In general, the findings in Figure 5 demonstrate that VeLU provides an effective alternative to standard activation functions, contributing to faster convergence and improved final model performance [22, 42].

### 3.3 Training Efficiency and Memory Usage

Table 4 compares activation functions across training time, inference speed, and memory usage. VeLU demonstrates consistently lower training loss, signaling more effective optimization [43, 44].

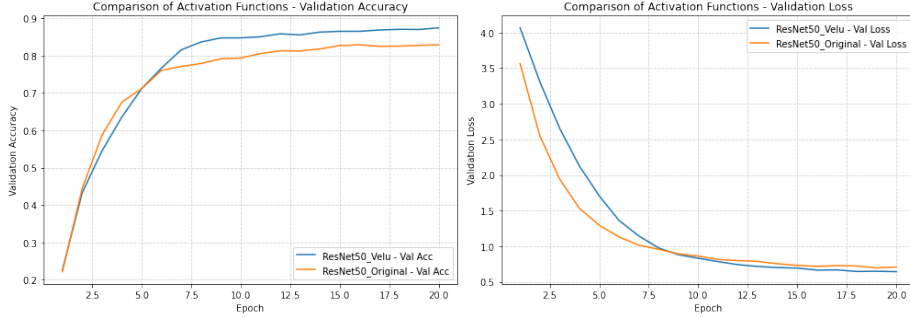


Figure 5: Comparison of VeLU vs. Original Activation in ResNet50. (Left) Validation accuracy over 20 epochs. (Right) Validation loss over the same period.

Compared to standard activations, VeLU achieves faster training in models like MobileNetV2 and ResNet50, and competitive performance in EfficientNetB3 and ViT-B16. The integration of adaptive scaling and regularization appears to improve training stability, particularly in lightweight and residual architectures. Inference performance also benefits from VeLU, notably in MobileNetV2 and EfficientNetB3, where it delivers higher FPS. Although GELU marginally outperforms VeLU in ViT-B16, the performance gap is small. Regarding memory usage, VeLU remains largely competitive, with slight increases in certain models likely due to more complex transformations. This is a common trade-off in adaptive activations [17].

Overall, Table 4 highlights VeLU’s strength in reducing training loss and improving inference speed while keeping memory overhead acceptable. These advantages position VeLU as a practical activation alternative, especially in resource-sensitive deployments.

Table 4: Performance comparison of various architectures with and without VeLU across different benchmarks. Loss, Training Time (s), Inference Speed (FPS), and Memory Usage (MB) are reported.

Model	Activation	Loss	Training Time (s)	FPS	Memory Usage (MB)
EfficientNetB3	VeLU	<b>0.4175</b>	2621.03	<b>16.07</b>	14786.01
	Swish [18]	0.4442	<b>2417.54</b>	15.16	<b>13403.34</b>
VGG19	VeLU	<b>0.3027</b>	<b>2047.57</b>	25.5	<b>14580.66</b>
	ReLU [8]	0.3702	2113.78	<b>28.65</b>	14730.04
ResNet50	VeLU	<b>0.3889</b>	1362.65	<b>20.2</b>	13704.64
	ReLU [8]	0.5318	<b>1353.11</b>	19.76	<b>13118.94</b>
MobileNetV2	VeLU	<b>0.3258</b>	<b>819.4</b>	<b>21.15</b>	14440.38
	ReLU6 [30]	0.3705	844.61	16.08	<b>13871.16</b>
DenseNet121	VeLU	<b>0.3153</b>	2246.35	15.78	<b>13628.08</b>
	ReLU [8]	0.4347	<b>1751.09</b>	<b>17.62</b>	13777.33
ViT_B16	VeLU	0.1436	692.38	11.29	<b>13259.38</b>
	GELU [5]	<b>0.1336</b>	<b>676.85</b>	<b>12.33</b>	13554.34

### 3.4 VeLU Behavior on Different Image Resolutions

Table 5 presents the performance of VeLU in different input resolutions in MobileNetV2 [12] on CIFAR-10 [32]. The results confirm that VeLU maintains stable performance across all tested resolutions, demonstrating adaptability to varying input scales. At  $32 \times 32$  resolution, VeLU achieves a test accuracy of 75.10%, indicating efficient learning even with low-resolution inputs. As resolution increases, accuracy improves consistently, reaching 93.34% at  $224 \times 224$  without signs of degradation. The top-5 accuracy remains above 98.5% across all resolutions, highlighting VeLU’s robust feature representation. This consistency can make VeLU particularly suitable for tasks where input sizes vary, such as transfer learning [36], medical imaging [45, 46], and real-time applications [47].

Table 5: Performance of VeLU on CIFAR-10 across different input resolutions using MobileNetV2.

Resolution	Top-1 Acc (%)	Top-5 Acc (%)
$32 \times 32$	75.10	98.51
$64 \times 64$	86.51	99.45
$128 \times 128$	91.32	99.70
$224 \times 224$	93.34	99.82

### 3.5 VeLU Adaptability With Different Optimizers

Table 6 presents the VeLU performance between different optimizers in ResNet50 in CIFAR-10 [32]. The results highlight VeLU’s adaptability across multiple optimization strategies. Adam, an adaptive gradient-based optimizer, enables VeLU to achieve a Top-1 accuracy of 91.32% and a Top-5 accuracy of 99.70% at  $128 \times 128$  resolution, showcasing its ability to generalize effectively. SGD, which relies on momentum-driven updates, achieves 89.33% Top-1 accuracy while maintaining a substantial 99.70% Top-5 accuracy, indicating VeLU’s stability even with conventional gradient descent methods. RMSProp, while slightly lower in performance (86.95% Top-1, 99.03% Top-5), further demonstrates VeLU’s adaptability by maintaining high recognition capability despite differences in gradient scaling and step size adjustments.

The ability of VeLU to perform consistently across different optimizers underscores its adaptability to varying training dynamics and model convergence behaviors. While Adam leads to achieving the highest accuracy, the close performance of SGD and RMSProp suggests that VeLU can be effectively trained under different optimization settings. These findings reinforce VeLU’s flexibility for deployment in real-world applications, where optimizer selection may depend on computational constraints or training efficiency [43, 61, 62].

Table 6: Performance of VeLU as a full replacement for ResNet50 activation functions on CIFAR-10 across different optimizers at  $128 \times 128$  resolution.

Optimizer	Top-1 Acc (%)	Top-5 Acc (%)
Adam	91.32	99.70
SGD	89.33	99.70
Nadam	87.23	99.19
RMSProp	86.95	99.03

## 4 Conclusion

In this work, we introduced VeLU, a novel activation function designed to improve the performance of deep neural networks by incorporating adaptive variance scaling, ArcTan-Sin transformations, and OT regularization. Extensive evaluations on CNNs and ViTs demonstrated that VeLU consistently enhances accuracy and improves generalization compared to ReLU, Swish, and GELU. Although VeLU incurs a slight increase in training time, its superior optimization stability and enhanced feature representation make it a compelling alternative for deep learning architectures, particularly in scenarios requiring robust gradient flow and efficient learning dynamics.

## References

- [1] V. Nair and G. E. Hinton, “Rectified Linear Units Improve Restricted Boltzmann Machines,” *Proceedings of the 27th International Conference on Machine Learning (ICML)*, pp. 807–814, 2010.
- [2] A. Krizhevsky, I. Sutskever, and G. E. Hinton, “ImageNet Classification with Deep Convolutional Neural Networks,” *Advances in Neural Information Processing Systems (NeurIPS)*, pp. 1097–1105, 2012.
- [3] A. L. Maas, A. Y. Hannun, and A. Ng, “Rectifier Nonlinearities Improve Neural Network Acoustic Models,” in *Proc. ICML Workshop on Deep Learning for Audio, Speech and Language Processing*, 2013.
- [4] D. Clevert, T. Unterthiner, and S. Hochreiter, “Fast and Accurate Deep Network Learning by Exponential Linear Units (ELUs),” *arXiv preprint [arXiv:1511.07289](#)*, 2015.
- [5] D. Hendrycks and K. Gimpel, “Gaussian Error Linear Units (GELUs),” *arXiv preprint [arXiv:1606.08415](#)*, 2016.
- [6] K. He, X. Zhang, S. Ren, and J. Sun, “Deep Residual Learning for Image Recognition,” *Proceedings of the IEEE Conference on Computer Vision and Pattern Recognition (CVPR)*, pp. 770–778, 2016.

- [7] A. Dosovitskiy et al., “An Image is Worth 16x16 Words: Transformers for Image Recognition at Scale,” *arXiv preprint [arXiv:2010.11929](#)*, 2020.
- [8] A. F. Agarap, “Deep Learning using Rectified Linear Units (ReLU),” *arXiv preprint [arXiv:1803.08375](#)*, 2018.
- [9] S. Ioffe and C. Szegedy, “Batch Normalization: Accelerating Deep Network Training by Reducing Internal Covariate Shift,” *Proceedings of the 32nd International Conference on Machine Learning (ICML)*, pp. 448–456, 2015.
- [10] P. Wolinski and J. Arbel, “Gaussian Pre-activations in Neural Networks: Myth or Reality?,” *arXiv preprint [arXiv:2205.12379](#)*, 2022.
- [11] M. Arjovsky, S. Chintala, and L. Bottou, “Wasserstein Generative Adversarial Networks,” *Proceedings of the 34th International Conference on Machine Learning (ICML)*, pp. 214–223, 2017.
- [12] M. Sandler, A. Howard, M. Zhu, A. Zhmoginov, and L.-C. Chen, “MobileNetV2: Inverted Residuals and Linear Bottlenecks,” *Proceedings of the IEEE Conference on Computer Vision and Pattern Recognition (CVPR)*, pp. 4510–4520, 2018.
- [13] G. Huang, Z. Liu, L. van der Maaten, and K. Q. Weinberger, “Densely Connected Convolutional Networks,” *Proceedings of the IEEE Conference on Computer Vision and Pattern Recognition (CVPR)*, pp. 4700–4708, 2017.
- [14] J. Ba, J. Kiros, and G. Hinton, “Layer Normalization,” *arXiv preprint [arXiv:1607.06450](#)*, 2016.
- [15] N. Courty, R. Flamary, A. Habrard, and A. Rakotomamonjy, “Joint Distribution Optimal Transportation for Domain Adaptation,” *Advances in Neural Information Processing Systems (NeurIPS)*, vol. 30, 2017.
- [16] E. F. Montesuma, F. M. N. Mboula, and A. Souloumiac, “Recent Advances in Optimal Transport for Machine Learning,” *IEEE Transactions on Pattern Analysis and Machine Intelligence*, 2024.
- [17] G. Klambauer, T. Unterthiner, A. Mayr, and S. Hochreiter, “Self-Normalizing Neural Networks,” *Advances in Neural Information Processing Systems (NeurIPS)*, vol. 30, 2017.
- [18] P. Ramachandran, B. Zoph, and Q. V. Le, “Searching for Activation Functions,” *arXiv preprint [arXiv:1710.05941](#)*, 2017.
- [19] X. Glorot, A. Bordes, and Y. Bengio, “Deep Sparse Rectifier Neural Networks,” *Proceedings of the 14th International Conference on Artificial Intelligence and Statistics (AISTATS)*, pp. 315–323, 2011.



- [20] W. Shang, K. Sohn, D. Almeida, and H. Lee, “Understanding and Improving Convolutional Neural Networks via Concatenated Rectified Linear Units,” *Proceedings of the 33rd International Conference on Machine Learning (ICML)*, pp. 2217–2225, 2016.
- [21] B. Xu, N. Wang, T. Chen, and M. Li, “Empirical Evaluation of Rectified Activations in Convolutional Network,” *arXiv preprint [arXiv:1505.00853](#)*, 2015.
- [22] H. Li, Z. Xu, G. Taylor, C. Studer, and T. Goldstein, “Visualizing the Loss Landscape of Neural Nets,” *Advances in Neural Information Processing Systems (NeurIPS)*, pp. 6391–6401, 2018.
- [23] R. Islamov, N. Ajroldi, A. Orvieto, and A. Lucchi, “Loss Landscape Characterization of Neural Networks without Over-Parametrization,” *arXiv preprint [arXiv:2410.12455](#)*, 2024.
- [24] N. S. Keskar, D. Mudigere, J. Nocedal, M. Smelyanskiy, and P. T. P. Tang, “On Large-Batch Training for Deep Learning: Generalization Gap and Sharp Minima,” *arXiv preprint [arXiv:1609.04836](#)*, 2016.
- [25] I. Goodfellow, Y. Bengio, and A. Courville, “Deep Learning,” MIT Press, 2016.
- [26] C. Villani, “Optimal Transport: Old and New,” vol. 338, pp. 129–131, Springer, Berlin, 2008.
- [27] J. Yosinski, J. Clune, Y. Bengio, and H. Lipson, “How Transferable are Features in Deep Neural Networks?,” *Advances in Neural Information Processing Systems (NeurIPS)*, pp. 3320–3328, 2014.
- [28] K. Simonyan and A. Zisserman, “Very Deep Convolutional Networks for Large-Scale Image Recognition,” *arXiv preprint [arXiv:1409.1556](#)*, 2014.
- [29] I. Gulrajani, F. Ahmed, M. Arjovsky, V. Dumoulin, and A. C. Courville, “Improved Training of Wasserstein GANs,” *Advances in Neural Information Processing Systems (NeurIPS)*, vol. 30, 2017.
- [30] A. G. Howard, M. Zhu, B. Chen, D. Kalenichenko, W. Wang, T. Weyand, M. Andreetto, and H. Adam, “MobileNets: Efficient Convolutional Neural Networks for Mobile Vision Applications,” *arXiv preprint [arXiv:1704.04861](#)*, 2017.
- [31] M. Lin, Q. Chen, and S. Yan, “Network In Network,” *arXiv preprint [arXiv:1312.4400](#)*, 2013.
- [32] A. Krizhevsky, “Learning Multiple Layers of Features from Tiny Images,” University of Toronto, Technical Report, 2009.

- [33] Y. LeCun, L. Bottou, Y. Bengio, and P. Haffner, “Gradient-Based Learning Applied to Document Recognition,” *Proceedings of the IEEE*, vol. 86, no. 11, pp. 2278–2324, 1998.
- [34] H. Xiao, K. Rasul, and R. Vollgraf, “Fashion-MNIST: A Novel Image Dataset for Benchmarking Machine Learning Algorithms,” *arXiv preprint [arXiv:1708.07747](#)*, 2017.
- [35] J. Z. Wang, J. Li, and G. Wiederhold, “SIMPLiCity: Semantics-Sensitive Integrated Matching for Picture Libraries,” *IEEE Transactions on Pattern Analysis and Machine Intelligence*, vol. 23, no. 9, pp. 947–963, 2001.
- [36] M. Tan and Q. V. Le, “EfficientNet: Rethinking Model Scaling for Convolutional Neural Networks,” *Proceedings of the 36th International Conference on Machine Learning (ICML)*, pp. 6105–6114, 2019.
- [37] C. Shorten and T. M. Khoshgoftaar, “A Survey on Image Data Augmentation for Deep Learning,” *Journal of Big Data*, vol. 6, no. 1, p. 60, 2019.
- [38] S. H. Gao, M. M. Cheng, K. Zhao, X. Y. Zhang, M. H. Yang, and P. Torr, “Res2Net: A New Multi-Scale Backbone Architecture,” *IEEE Transactions on Pattern Analysis and Machine Intelligence*, vol. 43, no. 2, pp. 652–662, 2019.
- [39] P. S. Hiremath and J. Pujari, “Content Based Image Retrieval Using Color, Texture and Shape Features,” in *Proceedings of the 15th International Conference on Advanced Computing and Communications (ADCOM)*, pp. 780–784, IEEE, 2007.
- [40] C. Zhang, S. Bengio, M. Hardt, B. Recht, and O. Vinyals, “Understanding Deep Learning Requires Rethinking Generalization,” *arXiv preprint [arXiv:1611.03530](#)*, 2016.
- [41] B. Neyshabur, S. Bhojanapalli, D. McAllester, and N. Srebro, “Exploring Generalization in Deep Learning,” *Advances in Neural Information Processing Systems (NeurIPS)*, vol. 30, 2017.
- [42] K. Kawaguchi, “Deep Learning Without Poor Local Minima,” *Advances in Neural Information Processing Systems (NeurIPS)*, vol. 29, 2016.
- [43] D. Kingma and J. Ba, “Adam: A Method for Stochastic Optimization,” *arXiv preprint [arXiv:1412.6980](#)*, 2014.
- [44] I. Loshchilov and F. Hutter, “Decoupled Weight Decay Regularization,” *arXiv preprint [arXiv:1711.05101](#)*, 2017.
- [45] G. Litjens, T. Kooi, B. Bejnordi, A. Setio, F. Ciompi, M. Ghafoorian, ... and J. van der Laak, “A Survey on Deep Learning in Medical Image Analysis,” *Medical Image Analysis*, vol. 42, pp. 60–88, 2017.

- [46] D. Shen, G. Wu, and H. Suk, “Deep Learning in Medical Image Analysis,” *Annual Review of Biomedical Engineering*, vol. 19, pp. 221-248, 2017.
- [47] A. Howard, M. Sandler, G. Chu, L.-C. Chen, B. Chen, M. Tan, ... and H. Adam, “Searching for MobileNetV3,” *Proceedings of the IEEE International Conference on Computer Vision (ICCV)*, pp. 1314-1324, 2019.
- [48] J. Deng, W. Dong, R. Socher, L. Li, K. Li, and L. Fei-Fei, “ImageNet: A Large-Scale Hierarchical Image Database,” *Proceedings of the IEEE Conference on Computer Vision and Pattern Recognition (CVPR)*, pp. 248-255, 2010.
- [49] Y. Bengio, “Practical Recommendations for Gradient-Based Training of Deep Architectures,” *Neural Networks: Tricks of the Trade*, pp. 437-478, 2012.
- [50] J. Bergstra and Y. Bengio, “Random Search for Hyper-Parameter Optimization,” *Journal of Machine Learning Research*, vol. 13, pp. 281-305, 2012.
- [51] M. Feurer and F. Hutter, “Hyperparameter Optimization,” *Automated Machine Learning*, pp. 3-33, 2019.
- [52] L. Li, K. Jamieson, G. DeSalvo, A. Rostamizadeh, and A. Talwalkar, “Hyperband: A Novel Bandit-Based Approach to Hyperparameter Optimization,” *Journal of Machine Learning Research*, 2017.
- [53] J. Bergstra, R. Bardenet, Y. Bengio, and B. Kégl, “Algorithms for Hyper-Parameter Optimization,” *Advances in Neural Information Processing Systems (NeurIPS)*, 2011.
- [54] J. Snoek, H. Larochelle, and R. P. Adams, “Practical Bayesian Optimization of Machine Learning Algorithms,” *Advances in Neural Information Processing Systems (NeurIPS)*, 2012.
- [55] C. Finn, P. Abbeel, and S. Levine, “Model-Agnostic Meta-Learning for Fast Adaptation of Deep Networks,” *Proceedings of the International Conference on Machine Learning (ICML)*, 2017.
- [56] T. Akiba, S. Sano, T. Yanase, T. Ohta, and M. Koyama, “Optuna: A Next-generation Hyperparameter Optimization Framework,” *Proceedings of the ACM SIGKDD International Conference on Knowledge Discovery and Data Mining*, 2019.
- [57] J. Bergstra, D. Yamins, and D. Cox, “Making a Science of Model Search: Hyperparameter Optimization in Hundreds of Dimensions for Vision Architectures,” *Proceedings of the International Conference on Machine Learning (ICML)*, 2013.

- [58] T. O'Malley, E. Bursztein, L. Long, F. Chollet, H. Jin, and others, "Keras Tuner," *GitHub repository*, 2019.
- [59] K. He, X. Zhang, S. Ren, and J. Sun, "Delving Deep into Rectifiers: Surpassing Human-Level Performance on ImageNet Classification," *Proceedings of the IEEE International Conference on Computer Vision (ICCV)*, pp. 1026–1034, 2015.
- [60] Y. Chen, X. Dai, M. Liu, D. Chen, L. Yuan, and Z. Liu, "Dynamic ReLU," in *Proceedings of the European Conference on Computer Vision (ECCV)*, pp. 351–367, Springer, Cham, 2020.
- [61] S. Ruder, "An Overview of Gradient Descent Optimization Algorithms," *arXiv preprint [arXiv:1609.04747](https://arxiv.org/abs/1609.04747)*, 2016.
- [62] G. Hinton, N. Srivastava, and K. Swersky, "Neural Networks for Machine Learning: Lecture 6a – Overview of Mini-Batch Gradient Descent," unpublished lecture notes, University of Toronto, 2012.